Directional Optical Sorting of Silicon Nanoparticles
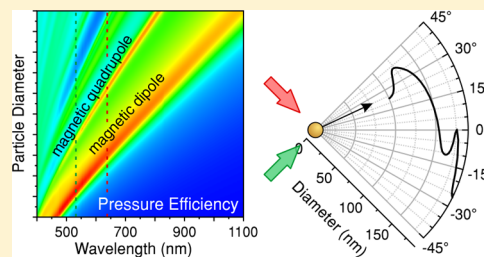
Daniil A. Shilkin,[†,‡] Evgeny V. Lyubin,[†] Maxim R. Shcherbakov,[†,§] Mikhail Lapine,[⊥] and Andrey A. Fedyanin*,[†]

[†]Faculty of Physics, Lomonosov Moscow State University, Moscow 119991, Russia
[‡]Center for Functionalized Magnetic Materials, Immanuel Kant Baltic Federal University, Kaliningrad 236041, Russia
[§]School of Applied and Engineering Physics, Cornell University, Ithaca, New York 14853, United States
[⊥]School of Mathematical and Physical Sciences, University of Technology Sydney, Sydney, NSW 2007, Australia

ABSTRACT: Optical manipulation of nanoparticles is a topic of great practical importance, with applications in surface science, colloidal chemistry, microfluidics, biochemistry, and medicine. One of the major highlights of this topic is particle sorting, which serves to create monodisperse systems remotely and to separate particles of different composition and size. Here, we analyze optical forces acting on spherical silicon nanoparticles that exhibit high-quality Mie resonances and demonstrate the potential of optical sorting methods for these systems. In particular, we propose multidirectional static sorting of nanoparticles using noncollinear beams with different wavelengths, which results in all-optical separation into an angular spectrum of sizes. We also validate the proposed methods by considering the operation in the presence of Brownian motion and in the evanescent wave configuration.

KEYWORDS: optical forces, optical sorting, Mie resonances, silicon nanoparticles

Silicon nanoparticles represent an emerging star in optics and photonics, as they produce high-quality resonances[1−10] with little dissipation,[11] benefit from biological compatibility,[12,13] and can be produced in commercial amounts at low cost. Their efficient usage has been reported in optical wavefront control,[14−16] harmonic generation,[17−20] optical switching,[21,22] and other applications. Silicon nanoparticles are typically produced by chemical methods,[9,23] nanosphere lithography combined with laser-induced transfer,[24] electron-beam lithography combined with reactive-ion etching,[6] or femtosecond laser ablation.[3−5,25] Even though some of the methodologies allow for a fairly homogeneous output in terms of particle size and shape, this comes at the cost of higher complexity and lower yield. In mass production, however, the output may often comprise a polydisperse mixture of different shapes and sizes, calling for a postproduction processing.

Separation of polydisperse particles by size can be achieved by a number of techniques including density-gradient centrifugation[26,27] and chromatographic filtering.[28] More recently, microfluidic methods started to be developed, being suitable for small-volume samples and direct integration with sterile, chemically pure, or hazardous environments.[29] Among them, optofluidic methods occupy a special place, providing high-throughput values and being more precise at a number of particular applications.[30]

To date, separation of particles by light can be accomplished by a variety of techniques, which are commonly divided into active and passive optical sorting. Active sorting implies automated closed-loop optical manipulation employing an external analysis of particle properties. Sorting of this kind has been realized with fluorescent activation[31,32] and Raman scattering analysis.[33] Passive sorting methods include optical chromatography,[34,35] cross-type optical chromatography,[36,37] near-field sorting based on a structural perturbation,[38] and more efficient and complicated sorting in interference patterns.[39−42] In the majority of reported experiments, separation of bidisperse suspensions was addressed. To handle polydisperse mixtures, a passive method with acousto-optically generated intensity patterns was developed[43] to sort particles of different sizes into four spatially separated streams. This technique, as the majority of passive sorting methods, employs fluid flow to transport the particles. On the other hand, motional optical patterns[40] or additional light pressure[41] enable flowless all-optical separation ("static" sorting), which can be utilized in isolated static environments.

More recently, intrinsic particle resonances have been exploited for optical sorting of particles. Strong dependence of the propulsion velocity on the particle size was observed for dielectric microspheres exhibiting high-quality whispering gallery modes.[44,45] A red shift of the plasmon resonance with increasing particle dimensions enables sorting of gold nanoparticles by size.[46−48] Theoretically, size-sensitive transverse optical force in a Gaussian beam[49] and negative scattering force in a Bessel beam[50] were proposed to sort plasmonic nanoparticles.

Contrary to plasmonic ones, high-permittivity dielectric nanoparticles did not receive significant research attention in

this context. In 2011, strong changes of radiation pressure on silicon and germanium nanospheres at the condition of the magnetic dipole resonance have been predicted theoretically.[51,52] During the last year, a great potential of optical forces for manipulation of single silicon nanoparticles has been demonstrated experimentally using optical tweezers[10] and numerically by considering optical binding forces.[53]

In this article, we analyze optical forces acting on spherical silicon nanoparticles exhibiting high-quality Mie resonances and demonstrate the potential of optical sorting methods for these systems. We propose a set of schemes for optical sorting of polydisperse silicon nanoparticle suspensions and discuss their practical potential by considering the operation in the presence of Brownian motion and in the evanescent wave configuration.

The general strategy underlying the proposed sorting techniques is illustrated by Figure 1. When a mixture of silicon
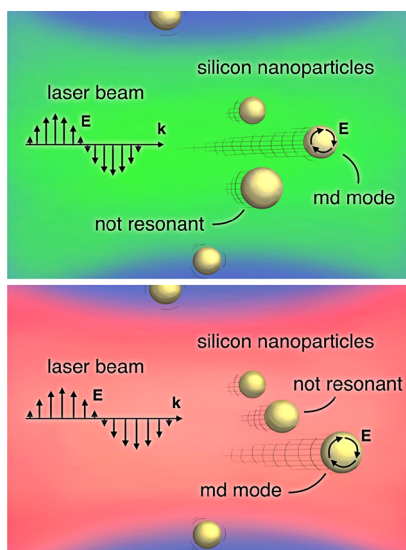

Figure 1. Artistic view of optically propelled silicon nanoparticles of various sizes in beams of different frequencies. Mie resonances excited in particles of certain sizes result in increased drift velocities in the direction of the laser beam propagation.

nanoparticles suspended in water is illuminated by laser beams, different Mie resonances are excited at different frequencies, depending on the particle size. The first resonance, a magnetic dipole, is excited when the particle diameter is approximately λ/n_i, where λ is the wavelength in a vacuum and n_i is the refractive index of the particle material. At larger particle sizes, the electric dipole and magnetic and electric quadrupoles are excited, in turn. When at resonance, the scattering efficiency and, in accordance with the momentum conservation law, the force acting on the particle are strongly enhanced, resulting in a higher drift velocity. In this way, the size of the particles propelled with higher velocities is controlled by the wavelength of the laser radiation, eventually allowing for efficient sorting mechanisms, described in the article.

■ SPECTRAL CHARACTERISTICS AND OPTICAL FORCES FOR SILICON NANOPARTICLES IN WATER

Light scattering by single particles is conveniently described by scattering and extinction efficiencies (Q_{sca}, Q_{ext}) determined as the corresponding cross sections normalized to the geometrical cross section of the particle. In Mie theory, scattering by a

spherical particle is described by an infinite series of the normal modes:[54]

$$Q_{sca} = \frac{2}{(kr)^2} \sum_{m=1}^{\infty} (2m+1)(|a_m|^2 + |b_m|^2) \tag{1}$$

$$Q_{ext} = \frac{2}{(kr)^2} \sum_{m=1}^{\infty} (2m+1)\mathrm{Re}(a_m + b_m) \tag{2}$$

where $k = 2\pi n_e/\lambda$ is the wavenumber in the surrounding medium (n_e is the medium refractive index, λ is the wavelength in a vacuum), r is the particle radius, and the coefficients a_m and b_m are calculated as follows:

$$a_m = \frac{n\psi_m(nkr)\,\psi_m'(kr) - \psi_m(kr)\,\psi_m'(nkr)}{n\psi_m(nkr)\,\xi_m'(kr) - \xi_m(kr)\,\psi_m'(nkr)} \tag{3}$$

$$b_m = \frac{\psi_m(nkr)\,\psi_m'(kr) - n\psi_m(kr)\,\psi_m'(nkr)}{\psi_m(nkr)\,\xi_m'(kr) - n\xi_m(kr)\,\psi_m'(nkr)} \tag{4}$$

where $n = n_i/n_e$ is the relative refractive index of the particle material, $\psi_m(\rho) = \rho j_m(\rho)$ and $\xi_m(\rho) = \rho h_m^{(1)}(\rho)$ are the Riccati−Bessel functions, $j_m(\rho)$ are the spherical Bessel functions of the first kind, and $h_m^{(1)}(\rho)$ are the spherical Hankel functions of the first kind.

The pressure on the particle is determined by the absorption and scattering efficiencies and the scattering directivity. In accordance with the momentum conservation law, when the particle scatters backward, the force is stronger than when it scatters in the forward direction. If the particle scatters forward in a nonparaxial optical field, the force can even change sign and start pulling the particle toward the light source.[42,50,55] In the case of plane waves, which is discussed in this article, the pressure efficiency Q_{pr} is found as follows:[54]

$$Q_{pr} = Q_{ext} - Q_{sca}\langle \cos\theta \rangle \tag{5}$$

where the asymmetry parameter is given by

$$Q_{sca}\langle \cos\theta \rangle =$$

$$\frac{4}{(kr)^2} \sum_m \frac{m(m+2)}{m+1}\mathrm{Re}(a_m a_{m+1}^* + b_m b_{m+1}^*)$$

$$+ \frac{4}{(kr)^2} \sum_m \frac{2m+1}{m(m+1)}\mathrm{Re}(a_m b_m^*) \tag{6}$$

Knowing the pressure efficiency, the force is calculated as $F = Q_{pr}\pi r^2 n_e I/c$, where I is the intensity of the plane wave illumination and c is the speed of light in a vacuum.

In contrast to most of the works on Mie resonances in silicon nanoparticles,[1−7] here we address scattering properties of silicon nanoparticles in water, as optical manipulation is commonly realized in an aqueous environment. Manipulation of nanoparticles in air is significantly more challenging because of higher turbulence, lower viscosity, and reduced heat dissipation.[56] The scattering spectrum calculated analytically for a 200 nm particle in water is shown in Figure 2a, as indicated by the purple curve; see Methods for details of the calculations. Although the quality of the resonances is not as high as in air, there is still a remarkable enhancement of scattering at the magnetic resonances. The extinction spectrum indicated in Figure 2a by the gray curve differs slightly from the scattering spectrum due to the low losses in silicon at visible
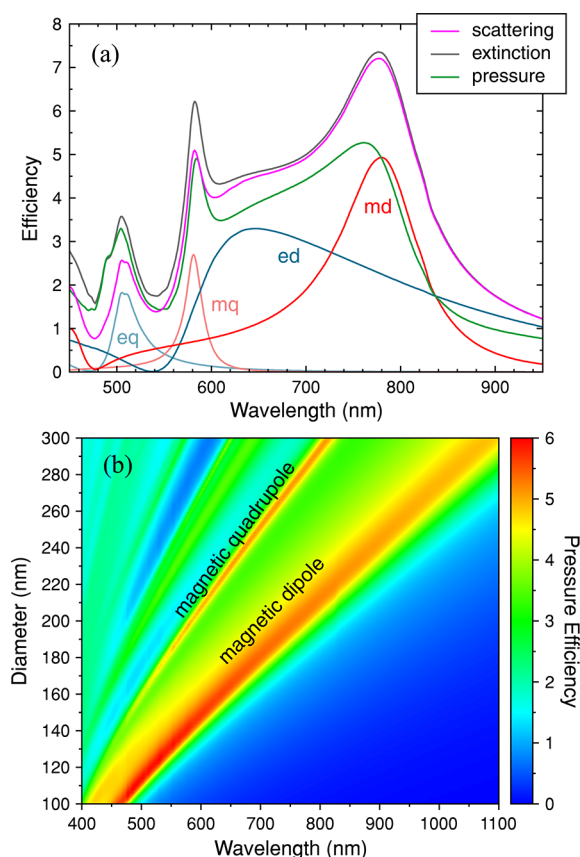
Figure 2. (a) Scattering, extinction, and pressure efficiencies calculated for a 200 nm silicon nanoparticle in water. Decomposition of the scattering efficiency into contributions of electric and magnetic dipoles (ed, md) and quadrupoles (eq, mq) is also shown. (b) Dependence of the pressure efficiency $Q_{pr} = F/(\pi r^2 n_c I/c)$ on the vacuum wavelength and the particle diameter calculated for a silicon sphere in water.
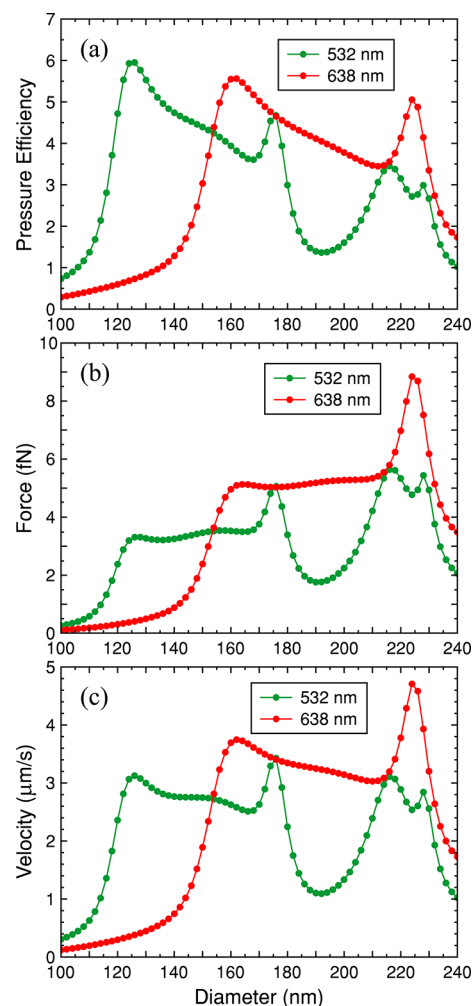

Figure 3. Size dependence of (a) the pressure efficiency, (b) the resulting force at a radiation intensity of 1 kW/cm², and (c) the corresponding propulsion velocity at wavelengths of 532 and 638 nm.

and near-infrared wavelengths. The calculated pressure efficiency is indicated in Figure 2a by the green curve. In Figure 2b, the pressure efficiency is given as a function of the particle size and the wavelength of the incident light. In this plot, the magnetic dipole and quadrupole resonances can be clearly identified for a broad range of particle dimensions, demonstrating a significant enhancement of the pressure efficiency at the resonances and a remarkable dependence on both the size and the wavelength that we propose to employ for sorting applications.

To illustrate the arising sorting scenarios, we consider two laser beams with typical wavelengths of 532 and 638 nm. We calculate how the pressure efficiency over a single nanoparticle (Figure 3a), the corresponding optical force (Figure 3b), and the arising velocity of its motion (Figure 3c) depend on the particle size. The steady-state particle drift velocity v under the action of the optical force is found from the balance with the viscous friction force, for which we employ Stoke's law $F = 6\pi\eta r v$, where η is the dynamic viscosity of water. The results presented in Figure 3 show essentially different size dependences for the two considered wavelengths, opening the route toward size separation.

■ OPTICAL SORTING METHODS

We now analyze three different schemes to employ these dependences for sorting of the nanoparticles according to their

resonance: (i) bidirectional sorting using counterpropagating laser beams, (ii) multidirectional sorting with the aid of a fluid flow in addition to the counterpropagating beams, and (iii) all-optical angular sorting using two orthogonal laser beams.

Bidirectional Sorting. For the first approach, the bidirectional sorting of nanoparticles, the suspension is subject to two laser beams of different frequencies propagating in opposite directions. A similar scheme was recently implemented for plasmonic nanoparticles.[47] In Figure 4a, we show the resulting drift velocity calculated as a function of the particle size for three sample scenarios with different ratios between the intensities of the two beams, I_g/I_r. To make an appropriate comparison, the total intensity is kept the same, *i.e.*, $I_g + I_r = 2$ kW/cm². From these results, it is clear that the sizes of nanoparticles can be distinguished according to their drift velocity. By varying the intensity ratio between the two beams, nanoparticles of certain sizes can be driven in opposite directions. For example, with the same intensity in the red beam I_r and the green beam I_g, particles smaller than 155 nm in diameter can be separated from the particles of larger than 155 nm size; note that particles of certain sizes will not systematically drift. This approach has certain limitations with regards to spatial sorting, as it is only the magnitude of the drift velocity that makes a distinction between different sizes within
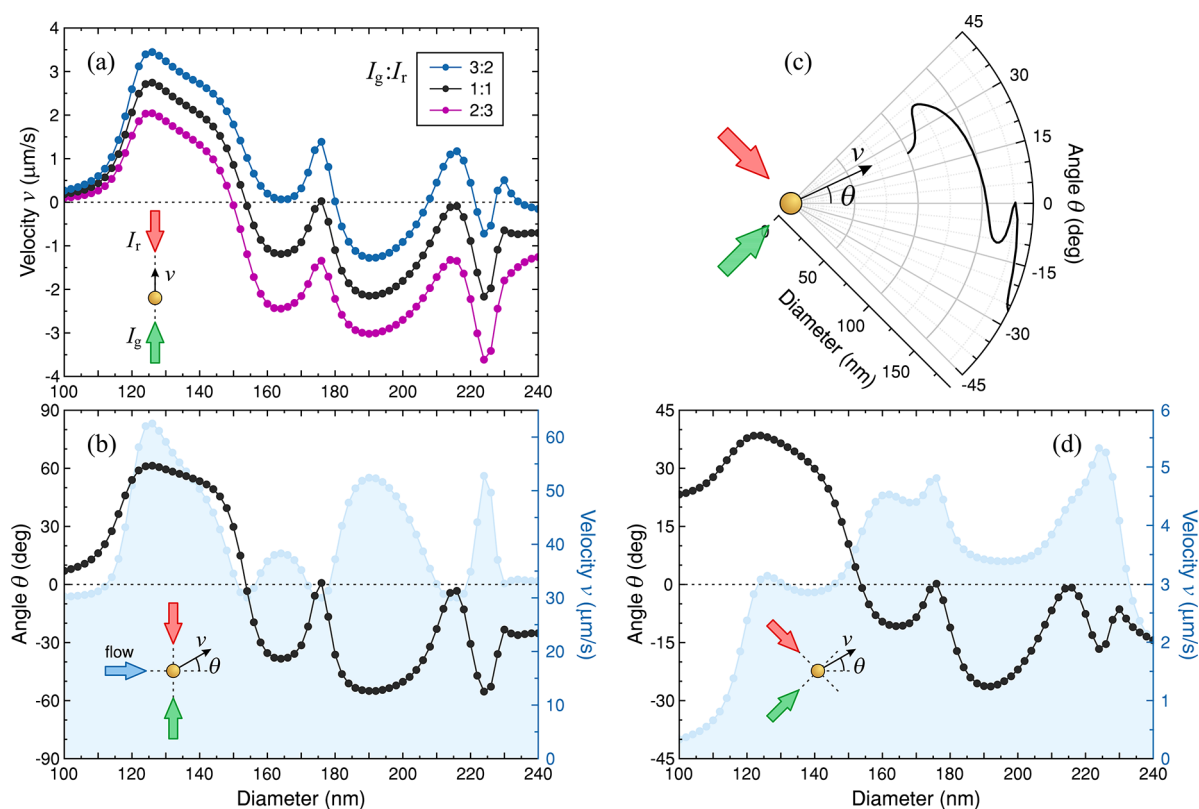
Figure 4. Optical sorting of silicon nanoparticles by two beams with vacuum wavelengths of 532 and 638 nm. (a) Bidirectional sorting in two counterpropagating plane waves with an average intensity of 1 kW/cm^2 and three different ratios of intensities. (b) Multidirectional sorting in two counterpropagating plane waves with intensities of 20 kW/cm^2 and a flow with a velocity of 30 μm/s. (c, d) Multidirectional static optical sorting in two perpendicular plane waves with intensities of 1 kW/cm^2.

a wide size range. As a more resolving opportunity, below we propose two methods for multidirectional sorting.

Multidirectional Sorting with a Liquid Flow. With two counterpropagating beams imposed over a uniform flow of a polydisperse mixture of nanoparticles, the particles of different sizes will deflect at different angles with respect to the original flow. To obtain broadly distributed angles of motion at reasonably distributed velocity magnitudes, the flow speed should be of the same order of magnitude as the characteristic light-driven drift velocities. An example of the resulting dependence of the deflection angle on the particle size, at a beam intensity of 20 kW/cm^2 and a flow velocity of 30 μm/s, is shown in Figure 4b. In this figure, we can identify certain size ranges, which can be efficiently separated. For example, particles with a 130−140 nm diameter will deflect to the left from the flow, whereas particles of 160−170 nm size will be driven to the right, with a clear correspondence between the deflection angle and the particle size.

In the shown example, a moderate flow rate is used. Using a faster flow would require higher light intensities or more complicated schemes, in which sorting is realized near a stagnation point, where the velocities are reduced.[57] Here we have considered a uniform flow and omitted the particle position distribution and the light and flow field gradients from consideration, as these parameters are dependent on the conditions of a particular realization.

All-Optical Angular Sorting. Our core proposal is to realize all-optical angular sorting. When the two beams with different frequencies are pointed at an angle, an efficient optical control over the particle drift direction can be realized without the use of an external suspension flow. In this case, larger particles experience a stronger optical force from the beam of a lower frequency, and smaller particles from the beam with a higher frequency. These forces are orthogonal to each other, with the ratio between the magnitudes of the two forces determined by the particle size. As a consequence, a particle with a given size will be moving at a specific angle between the two beams.

We illustrate the power of this approach by imposing the 532 and 638 nm beams perpendicular to each other. The resulting dependence of the drift direction on the particle size is shown in Figure 4c on a polar plot for a clear visualization, whereas Figure 4d presents the same dependence, as well as that of the drift velocity, on a standard plot. For certain size ranges, there is a unique correspondence between the size and the direction, and a disperse mixture of particles is conveniently separated into an angular spectrum of sizes. In this case, particles in a wide size range between 120 and 160 nm (as well as those between 190 and 215 nm) can be clearly separated according to their drift direction and velocity.

Generalizing the above example, we conclude that, depending on the choice of the laser frequencies, there is a range of particle sizes where a unique correspondence between the particle size and the drift angle can be established. That range and, accordingly, the separation precision can be controlled by choosing the handling frequencies and the angle between the beams.

Finally, we would like to note that the proposed sorting schemes rely on the spectral position of the resonances and may therefore be suitable not only for size separation but also

for sorting nanoparticles according to their shape, particularly for elongated[58] or oblate particles,[10] as the resonances are strongly affected by shape.[2,6] However, further extended analysis will be required to fully evaluate the arising opportunities.

ROLE OF THE BROWNIAN MOTION

So far, we did not account for Brownian motion, although this is an important factor determining the actual resolution of the separation techniques. We now analyze the influence of Brownian motion, based on standard methods (see Methods for details).

In order to illustrate how the Brownian motion at room temperature affects the proposed techniques, we model the separation of nanoparticles of three different sizes (130, 150, and 160 nm in diameter) in the angular sorting scheme by two perpendicular laser beams, 532 and 638 nm, with intensities of 1 kW/cm^2. The numerically simulated sample trajectories of the particles sorted from the same original position are shown in Figure 5, as indicated by the solid curves. During the process,
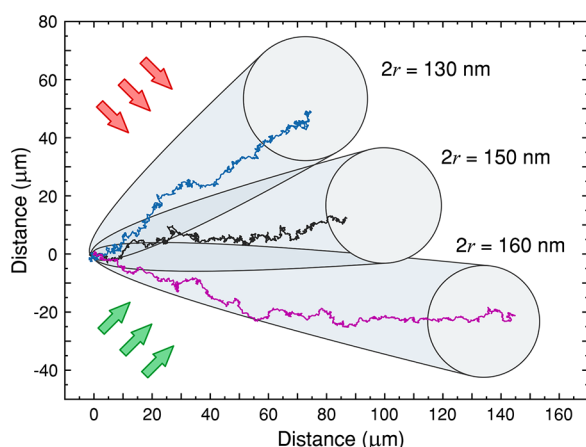

Figure 5. Multidirectional static optical sorting of 130, 150, and 160 nm silicon spheres in water, affected by Brownian motion. For calculations, two perpendicular plane waves with intensities of 1 kW/cm^2 and wavelengths of 532 and 638 nm are assumed. The trajectories are shown with thin colored curves, for the motion time of 30 s. The filled circles show the standard deviation of the final positions, and the filled parabolic contours correspond to the standard deviation for the intermediate positions.

the particles drift with constant velocities determined by the optical forces and are stochastically displaced from the mean position in accordance with Einstein's theory of Brownian motion. The analytically derived standard deviations of the final positions upon a 30 s sorting process are shown in Figure 5 with the gray circles, and the standard deviations during the process are shown with the corresponding parabolic contours. It can be noticed that the circle corresponding to the largest particle is the smallest, as it is less affected by Brownian motion.

We can conclude that, in this example, a reliable separation between those three sizes is achieved upon a 30 s process. The required optical power, which is the intensity times the separation distance scale squared, is approximately 0.1 W, which is less than the typical power for experiments on passive optical sorting,[37,39−43,47] and, therefore, the proposed method is experimentally plausible and represents a promising alternative.

SORTING WITH AN EVANESCENT SETUP

The results reported above were obtained assuming plane wave radiation. However, the majority of experiments on optical sorting are performed in the evanescent wave configuration, when a beam used for manipulation is incident from outside of the liquid interface so as to undergo a total internal reflection, whereas the particles on the other side of the interface are trapped with the resulting evanescent fields.[59−61] To confine the particles within the volume close to the surface, where they can best interact with the radiation, gravity[37] or, for a better precision, hydrodynamic focusing[62] can be used.

To clarify how our proposals are affected in this scenario, we have performed finite difference time domain (FDTD) simulations over a silicon particle located in the field of an evanescent wave; see Methods for details of the simulations. In the model, a light pulse propagating in a medium with a refractive index of 1.5 is incident on an interface with water at an angle of incidence of 65°. Then the Fourier components of the electromagnetic field are determined at the frequencies of interest. For all the simulations, the gap between the surface and the particle was set to 50 nm, while the diameter of the silicon sphere was varied.

The results of the numerical calculations for two polarizations of the incident light are given in Figure 6 in comparison with the analytical solutions for plane wave illumination shown in the background in Figure 6a. Besides the higher absolute values due to the enhancement of the field at the interface,[63] the size dependence of the force in the direction of propagation of the evanescent wave shows the same behavior as the dependence for plane wave illumination. One can conclude, therefore, that at a constant distance between the particle and the surface, the results above are fully applicable for the evanescent field configuration.

The distance between the particle and the surface can remain constant if there is a stable equilibrium position in the vicinity of the surface. This is usually realized by the balance of the gradient optical force pulling the particle to the surface and a short-range repulsive static electric force. However, due to the excitation of the resonances, silicon nanoparticles are not always attracted to the interface, as a dipole would. The force component perpendicular to the surface is shown in Figure 6b and demonstrates that either attraction or repulsion is observed, depending on the size, polarization, and wavelength. For instance, in the case of s-polarized illumination, a pulling force is observed when the particle size is slightly smaller than the size corresponding to the magnetic dipole resonance at a given wavelength (157 nm for 638 nm wavelength and 122 nm for 532 nm wavelength), whereas a repulsive force is observed for the size above that resonance. This Fano-like behavior can be explained if one considers the Mie resonator as a driven oscillator, which experiences a π-shift of the oscillation phase when the driving frequency is equal to the intrinsic oscillator frequency. When the size of the particle is smaller than the resonant size, the light frequency is smaller than the resonant one, and the induced magnetic dipole moment oscillates in phase with the external magnetic field. In this case, the particle experiences a gradient force directed to the surface. When the particle size is bigger than the resonant one, the induced magnetic dipole moment oscillates in antiphase with the field, so the repulsion takes place. Note that the effect can be observed in either polarization, but is more pronounced with s-
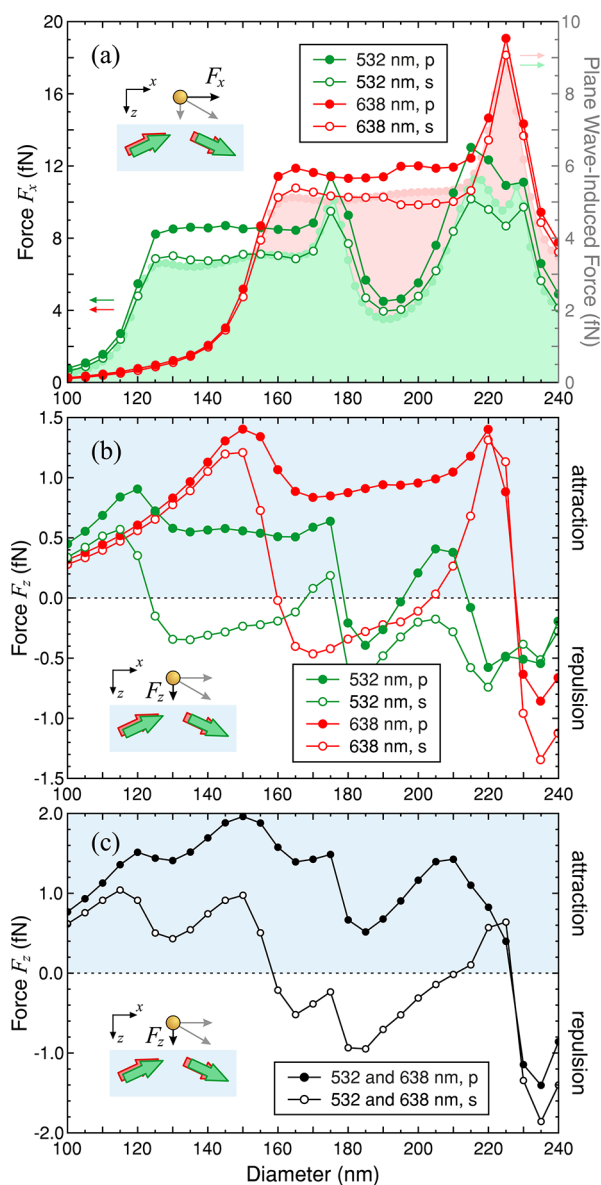
Figure 6. Numerically calculated force induced by an evanescent wave formed in the vicinity of the interface between a dielectric with a refractive index of 1.5 and water by light with an intensity of 1 kW/cm^2 incident upon an angle of 65°. The gap between the surface and the particle is 50 nm. (a) Tangential component of the force. Plane-wave-induced force at the same intensity is given on the background. (b) Normal component. In the region depicted by the blue area, particles are attracted to the surface and the sorting methods discussed can be applied in the evanescent configuration. (c) Total normal component in the case of illumination by the two waves with the same intensity (1 kW/cm^2 each).

polarized illumination because in this case the induced dipole moment is directed perpendicular to the gradient of the field.

For the intended angular sorting with two beams, it is required that the total F_z force is positive, which corresponds to the shaded area in Figure 6c. Generally, p-polarization appears entirely suitable, with the particles up to 220 nm attracted to the surface; for s-polarization, sorting is only possible for sizes below 155 nm. In particular, the entire scenario shown in Figure 5 can be realized in the evanescent configuration using p-polarized illumination. Outside of the mentioned size ranges, the net optical force will push the particles away from the

surface, making evanescent sorting impossible. As a side comment, we note that repulsion from the surface in the evanescent configuration is not observed with low-contrast particles of submicrometer dimensions,[60,64] as the resonances are not excited, which can also potentially be utilized for optical sorting.

CONCLUSION

In summary, we have presented a parametric analysis of the optical forces acting on high-permittivity silicon nanoparticles in water, depending on their size and the wavelength of the incident radiation. On the basis of these results, we have shown the potential of applying these forces to achieve optical sorting of nanoparticles according to their resonances using a combination of laser beams and, optionally, mechanical flow. In particular, we proposed a novel technique of all-optical multidirectional separation of nanoparticles using noncollinear beams of different wavelengths. We have shown that the proposed method becomes robust against Brownian motion at a modest optical power of 0.1 W and can resolve nanoparticles of about 150 nm diameter with a 10 nm difference in size. We have also demonstrated that the proposed approaches remain suitable in the evanescent field configuration at a broad range of particle dimensions using p-polarized illumination. We anticipate that the reported results will lead to experimental implementations, bringing fundamental improvements to practical nanosorting techniques.

METHODS

Analytical Calculations. For the calculations performed, the dispersion of the dielectric permittivity of silicon[11,65] and the real part of the refractive index of water[66] were used. The imaginary part of the refractive index of water was neglected, as it is at least 5 orders smaller in the region of interest than the real one.[67] In the series 1 and 2, only the first three terms were taken into account ($m \leq 3$) as the other terms are at least 5 orders of magnitude smaller.

Modeling Brownian Motion. The sample trajectories shown in Figure 5 by the colored curves were obtained by finite-difference simulations based on the overdamped Langevin equation. The method is described, for example, in ref 68. In the simulations, the constant optical force was set in accordance with the results of the analytical analysis, whereas the random component was generated using the extended cellular automatic algorithm in Wolfram Mathematica software.

The regions illustrating the standard deviation were obtained using Einstein's theory of Brownian motion. For two-dimensional probability densities, as relevant for the example discussed, the standard deviation of the radial coordinate is determined by the following relation:

$$\sigma^2 = \overline{(x - v_x t)^2} + \overline{(y - v_y t)^2} = 4Dt \tag{7}$$

where $D = k_B T/(6\pi\eta r)$ is the diffusion coefficient, k_B is the Boltzmann constant, and T is the temperature. The radii of the filled circles in Figure 6 are equal to $\sigma|_{t=30s}$. The parabolic contours show how the standard deviation evolves during the process. If a particle drifts along the x-axis, the corresponding parabola is given by the equation $y^2 = 4D/v(x + D/v)$.

Finite-Difference Time-Domain Simulations. The FDTD simulations were performed using Lumerical FDTD Solutions software. The simulated region was $4 \times 4 \times 2$ μm^3 in size, with the shorter side perpendicular to the interface. The

boundary conditions were set to the Bloch ones for the facets perpendicular to the interface and to perfectly matched layers for the other two sides. A silicon sphere was placed in the center of the simulated region. The absence of possible coupling effects due to the periodic boundary conditions was verified by varying the size of the simulation region. A plane wave incident from the dielectric with a refractive index of 1.5 was used as the light source. Upon the simulation of the light pulse propagation, the Fourier components of the electromagnetic field were determined at the frequencies of interest. The force acting on the particle was subsequently found by integrating the Maxwell stress tensor components over a surface enclosing the particle and normalized to the intensity of the incident radiation of 1 kW/cm^2.

■ AUTHOR INFORMATION

Corresponding Author

*E-mail: fedyanin@nanolab.phys.msu.ru.

ORCID Ⓞ

Andrey A. Fedyanin: 0000-0003-4708-6895

Notes

The authors declare no competing financial interest.

■ REFERENCES

(1) Evlyukhin, A. B.; Reinhardt, C.; Seidel, A.; Luk'yanchuk, B. S.; Chichkov, B. N. Optical response features of Si-nanoparticle arrays. *Phys. Rev. B: Condens. Matter Mater. Phys.* **2010**, *82*, 045404.

(2) Evlyukhin, A. B.; Reinhardt, C.; Chichkov, B. N. Multipole light scattering by nonspherical nanoparticles in the discrete dipole approximation. *Phys. Rev. B: Condens. Matter Mater. Phys.* **2011**, *84*, 235429.

(3) Evlyukhin, A. B.; Novikov, S. M.; Zywietz, U.; Eriksen, R. L.; Reinhardt, C.; Bozhevolnyi, S. I.; Chichkov, B. N. Demonstration of magnetic dipole resonances of dielectric nanospheres in the visible region. *Nano Lett.* **2012**, *12*, 3749−3755.

(4) Kuznetsov, A. I.; Miroshnichenko, A. E.; Fu, Y. H.; Zhang, J.; Luk'yanchuk, B. Magnetic light. *Sci. Rep.* **2012**, *2*, 492.

(5) Zywietz, U.; Evlyukhin, A. B.; Reinhardt, C.; Chichkov, B. N. Laser printing of silicon nanoparticles with resonant optical electric and magnetic responses. *Nat. Commun.* **2014**, *5*, 3402.

(6) Staude, I.; Miroshnichenko, A. E.; Decker, M.; Fofang, N. T.; Liu, S.; Gonzales, E.; Dominguez, J.; Luk, T. S.; Neshev, D. N.; Brener, I.; Kivshar, Yu. Tailoring directional scattering through magnetic and electric resonances in subwavelength silicon nanodisks. *ACS Nano* **2013**, *7*, 7824−7832.

(7) Li, S.; Song, W.; Crozier, K. B. Isolated and collective magnetic resonances in dielectric nanoparticles at optical frequencies. CLEO: QELS_Fundamental Science 2016, FM4B.3.

(8) Shi, L.; Tuzer, T. U.; Fenollosa, R.; Meseguer, F. A new dielectric metamaterial building block with a strong magnetic response in the sub-1.5-micrometer region: silicon colloid nanocavities. *Adv. Mater.* **2012**, *24*, 5934−5938.

(9) Shi, L.; Harris, J. T.; Fenollosa, R.; Rodriguez, I.; Lu, X.; Korgel, B. A.; Meseguer, F. Monodisperse silicon nanocavities and photonic crystals with magnetic response in the optical region. *Nat. Commun.* **2013**, *4*, 1904.

(10) Andres-Arroyo, A.; Gupta, B.; Wang, F.; Gooding, J. J.; Reece, P. J. Optical manipulation and spectroscopy of silicon nanoparticles exhibiting dielectric resonances. *Nano Lett.* **2016**, *16*, 1903−1910.

(11) Aspnes, D. E.; Studna, A. A. Dielectric functions and optical parameters of Si, Ge, GaP, GaAs, GaSb, InP, InAs, and InSb from 1.5 to 6.0 eV. *Phys. Rev. B: Condens. Matter Mater. Phys.* **1983**, *27*, 985−1009.

(12) Erogbogbo, F.; Yong, K.-T.; Roy, I.; Xu, G.; Prasad, P. N.; Swihart, M. T. Biocompatible luminescent silicon quantum dots for imaging of cancer cells. *ACS Nano* **2008**, *2*, 873−878.

(13) Bimbo, L. M.; Sarparanta, M.; Santos, H. A.; Airaksinen, A. J.; Mäkilä, E.; Laaksonen, T.; Peltonen, L.; Lehto, V.-P.; Hirvonen, J.; Salonen, J. Biocompatibility of thermally hydrocarbonized porous silicon nanoparticles and their biodistribution in rats. *ACS Nano* **2010**, *4*, 3023−3032.

(14) Shalaev, M. I.; Sun, J.; Tsukernik, A.; Pandey, A.; Nikolskiy, K.; Litchinitser, N. M. High-efficiency all-dielectric metasurfaces for ultracompact beam manipulation in transmission mode. *Nano Lett.* **2015**, *15*, 6261−6266.

(15) Yu, Y. F.; Zhu, A. Y.; Paniagua-Domínguez, R.; Fu, Y. H.; Luk'yanchuk, B.; Kuznetsov, A. I. High-transmission dielectric metasurface with 2π phase control at visible wavelengths. *Laser Photon. Rev.* **2015**, *9*, 412−418.

(16) Chong, K. E.; Wang, L.; Staude, I.; James, A. R.; Dominguez, J.; Liu, S.; Subramania, G. S.; Decker, M.; Neshev, D. N.; Brener, I.; Kivshar, Y. S. Efficient polarization-insensitive complex wavefront control using Huygens' metasurfaces based on dielectric resonant meta-atoms. *ACS Photonics* **2016**, *3*, 514−519.

(17) Shcherbakov, M. R.; Neshev, D. N.; Hopkins, B.; Shorokhov, A. S.; Staude, I.; Melik-Gaykazyan, E. V.; Decker, M.; Ezhov, A. A.; Miroshnichenko, A. E.; Brener, I.; Fedyanin, A. A.; Kivshar, Y. S. Enhanced third-harmonic generation in silicon nanoparticles driven by magnetic response. *Nano Lett.* **2014**, *14*, 6488−6492.

(18) Yang, Y.; Wang, W.; Boulesbaa, A.; Kravchenko, I. I.; Briggs, D. P.; Puretzky, A.; Geohegan, D.; Valentine, J. Nonlinear Fano-resonant dielectric metasurfaces. *Nano Lett.* **2015**, *15*, 7388−7393.

(19) Shorokhov, A. S.; Melik-Gaykazyan, E. V.; Smirnova, D. A.; Hopkins, B.; Chong, K. E.; Choi, D.-Y.; Shcherbakov, M. R.; Miroshnichenko, A. E.; Neshev, D. N.; Fedyanin, A. A.; Kivshar, Y. S. Multifold enhancement of third-harmonic generation in dielectric nanoparticles driven by magnetic Fano resonances. *Nano Lett.* **2016**, *16*, 4857−4861.

(20) Melik-Gaykazyan, E. V.; Shcherbakov, M. R.; Shorokhov, A. S.; Staude, I.; Brener, I.; Neshev, D. N.; Kivshar, Y. S.; Fedyanin, A. A. Third-harmonic generation from Mie-type resonances of isolated all-dielectric nanoparticles. *Philos. Trans. R. Soc., A* **2017**, *375*, 20160281.

(21) Shcherbakov, M. R.; Vabishchevich, P. P.; Shorokhov, A. S.; Chong, K. E.; Choi, D.-Y.; Staude, I.; Miroshnichenko, A. E.; Neshev, D. N.; Fedyanin, A. A.; Kivshar, Y. S. Ultrafast all-optical switching with magnetic resonances in nonlinear dielectric nanostructures. *Nano Lett.* **2015**, *15*, 6985−6990.

(22) Baranov, D. G.; Makarov, S. V.; Milichko, V. A.; Kudryashov, S. I.; Krasnok, A. E.; Belov, P. A. Nonlinear transient dynamics of photoexcited resonant silicon nanostructures. *ACS Photonics* **2016**, *3*, 1546−1551.

(23) Pell, L. E.; Schricker, A. D.; Mikulec, F. V.; Korgel, B. A. Synthesis of amorphous silicon colloids by trisilane thermolysis in high temperature supercritical solvents. *Langmuir* **2004**, *20*, 6546−6548.

(24) Kuznetsov, A. I.; Evlyukhin, A. B.; Gonçalves, M. R.; Reinhardt, C.; Koroleva, A.; Arnedillo, M. L.; Kiyan, R.; Marti, O.; Chichkov, B. N. Laser fabrication of large-scale nanoparticle arrays for sensing applications. *ACS Nano* **2011**, *5*, 4843−4849.

(25) Kuzmin, P. G.; Shafeev, G. A.; Bukin, V. V.; Garnov, S. V.; Farcau, C.; Carles, R.; Warot-Fontrose, B.; Guieu, V.; Viau, G. Silicon nanoparticles produced by femtosecond laser ablation in ethanol: size control, structural characterization, and optical properties. *J. Phys. Chem. C* **2010**, *114*, 15266−15273.

(26) Kowalczyk, B.; Lagzi, I.; Grzybowski, B. A. Nanoseparations: strategies for size and/or shape-selective purification of nanoparticles. *Curr. Opin. Colloid Interface Sci.* **2011**, *16*, 135−148.

(27) Mastronardi, M. L.; Hennrich, F.; Henderson, E. J.; Maier-Flaig, F.; Blum, C.; Reichenbach, J.; Lemmer, U.; Kübel, C.; Wang, D.; Kappes, M. M.; Ozin, G. A. Preparation of monodisperse silicon nanocrystals using density gradient ultracentrifugation. *J. Am. Chem. Soc.* **2011**, *133*, 11928−11931.

(28) Contado, C.; Argazzi, R. Size sorting of citrate reduced gold nanoparticles by sedimentation field-flow fractionation. *J. Chromatogr. A* **2009**, *1216*, 9088−9098.

(29) Sajeesh, P.; Sen, A. K. Particle separation and sorting in microfluidic devices: a review. *Microfluid. Nanofluid.* **2014**, *17*, 1−52.

(30) Jonáš, A.; Zemánek, P. Light at work: The use of optical forces for particle manipulation, sorting, and analysis. *Electrophoresis* **2008**, *29*, 4813−4851.

(31) Wang, M. M.; Tu, E.; Raymond, D. E.; Yang, J. M.; Zhang, H.; Hagen, N.; Dees, B.; Mercer, E. M.; Forster, A. H.; Kariv, I.; Marchand, Ph. J; Butler, W. F. Microfluidic sorting of mammalian cells by optical force switching. *Nat. Biotechnol.* **2005**, *23*, 83−87.

(32) Applegate, R. W., Jr.; Squier, J.; Vestad, T.; Oakey, J.; Marr, D. W. M.; Bado, P.; Dugan, M. A.; Said, A. A. Microfluidic sorting system based on optical waveguide integration and diode laser bar trapping. *Lab Chip* **2006**, *6*, 422−426.

(33) Lau, A. Y.; Lee, L. P.; Chan, J. W. An integrated optofluidic platform for Raman-activated cell sorting. *Lab Chip* **2008**, *8*, 1116−1120.

(34) Imasaka, T.; Kawabata, Y.; Kaneta, T.; Ishidzu, Y. Optical chromatography. *Anal. Chem.* **1995**, *67*, 1763−1765.

(35) Hatano, T.; Kaneta, T.; Imasaka, T. Application of optical chromatography to immunoassay. *Anal. Chem.* **1997**, *69*, 2711−2715.

(36) Kim, S. B.; Kim, J. H.; Kim, S. S. Theoretical development of in situ optical particle separator: cross-type optical chromatography. *Appl. Opt.* **2006**, *45*, 6919−6924.

(37) Marchington, R. F.; Mazilu, M.; Kuriakose, S.; Garcés-Chávez, V.; Reece, P. J.; Krauss, T. F.; Gu, M.; Dholakia, K. Optical deflection and sorting of microparticles in a near-field optical geometry. *Opt. Express* **2008**, *16*, 3712−3726.

(38) Lin, S.; Crozier, K. B. An integrated microparticle sorting system based on near-field optical forces and a structural perturbation. *Opt. Express* **2012**, *20*, 3367−3374.

(39) MacDonald, M. P.; Spalding, G. C.; Dholakia, K. Microfluidic sorting in an optical lattice. *Nature* **2003**, *426*, 421−424.

(40) Čižmár, T.; Šiler, M.; Šerý, M.; Zemánek, P.; Garcés-Chávez, V.; Dholakia, K. Optical sorting and detection of submicrometer objects in a motional standing wave. *Phys. Rev. B: Condens. Matter Mater. Phys.* **2006**, *74*, 035105.

(41) Jákl, P.; Čižmár, T.; Šerý, M.; Zemánek, P. Static optical sorting in a laser interference field. *Appl. Phys. Lett.* **2008**, *92*, 161110.

(42) Brzobohatý, O.; Karásek, V.; Šiler, M.; Chvátal, L.; Čižmár, T.; Zemánek, P. Experimental demonstration of optical transport, sorting and self-arrangement using a 'tractor beam'. *Nat. Photonics* **2013**, *7*, 123−127.

(43) Milne, G.; Rhodes, D.; MacDonald, M.; Dholakia, K. Fractionation of polydisperse colloid with acousto-optically generated potential energy landscapes. *Opt. Lett.* **2007**, *32*, 1144−1146.

(44) Li, Y.; Svitelskiy, O. V.; Maslov, A. V.; Carnegie, D.; Rafailov, E.; Astratov, V. N. Giant resonant light forces in microspherical photonics. *Light: Sci. Appl.* **2013**, *2*, e64.

(45) Li, Y.; Maslov, A. V.; Limberopoulos, N. I.; Urbas, A. M.; Astratov, V. N. Spectrally resolved resonant propulsion of dielectric microspheres. *Laser Photon. Rev.* **2015**, *9*, 263−273.

(46) Ploschner, M.; Mazilu, M.; Čižmár, T.; Dholakia, K. Numerical investigation of passive optical sorting of plasmon nanoparticles. *Opt. Express* **2011**, *19*, 13922−13933.

(47) Ploschner, M.; Čižmár, T.; Mazilu, M.; di Falco, A.; Dholakia, K. Bidirectional optical sorting of gold nanoparticles. *Nano Lett.* **2012**, *12*, 1923−1927.

(48) Cuche, A.; Canaguier-Durand, A.; Devaux, E.; Hutchison, J. A.; Genet, C.; Ebbesen, T. W. Sorting nanoparticles with intertwined plasmonic and thermo-hydrodynamical forces. *Nano Lett.* **2013**, *13*, 4230−4235.

(49) Li, Z.; Zhang, S.; Tong, L.; Wang, P.; Dong, B.; Xu, H. Ultrasensitive size-selection of plasmonic nanoparticles by Fano interference optical force. *ACS Nano* **2013**, *8*, 701−708.

(50) Chen, H.; Liu, S.; Zi, J.; Lin, Z. Fano resonance-induced negative optical scattering force on plasmonic nanoparticles. *ACS Nano* **2015**, *9*, 1926−1935.

(51) Nieto-Vesperinas, M.; Gomez-Medina, R.; Saenz, J. J. Angle-suppressed scattering and optical forces on submicrometer dielectric particles. *J. Opt. Soc. Am. A* **2011**, *28*, 54−60.

(52) Gómez-Medina, R.; García-Cámara, B.; Suárez-Lacalle, I.; González, F.; Moreno, F.; Nieto-Vesperinas, M.; Sáenz, J. J. Electric and magnetic dipolar response of germanium nanospheres: interference effects, scattering anisotropy, and optical forces. *J. Nanophotonics* **2011**, *5*, 053512.

(53) Yano, T. A.; Tsuchimoto, Y.; Zaccaria, R. P.; Toma, A.; Portela, A.; Hara, M. Enhanced optical magnetism for reversed optical binding forces between silicon nanoparticles in the visible region. *Opt. Express* **2017**, *25*, 431−439.

(54) Bohren, C. F.; Huffman, D. R. *Absorption and Scattering of Light by Small Particles*; John Wiley & Sons, 2008.

(55) Chen, J.; Ng, J.; Lin, Z.; Chan, C. T. Optical pulling force. *Nat. Photonics* **2011**, *5*, 531−534.

(56) Jauffred, L.; Taheri, S. M.-R.; Schmitt, R.; Linke, H.; Oddershede, L. B. Optical trapping of gold nanoparticles in air. *Nano Lett.* **2015**, *15*, 4713−4719.

(57) Wu, W.; Zhu, X.; Zuo, Y.; Liang, L.; Zhang, S.; Zhang, X.; Yang, Y. Precise sorting of gold nanoparticles in a flowing system. *ACS Photonics* **2016**, *3*, 2497−2504.

(58) Toe, W. J.; Ortega-Piwonka, I.; Angstmann, C. N.; Gao, Q.; Tan, H. H.; Jagadish, C.; Henry, B. I.; Reece, P. J. Nonconservative dynamics of optically trapped high-aspect-ratio nanowires. *Phys. Rev. E: Stat. Phys., Plasmas, Fluids, Relat. Interdiscip. Top.* **2016**, *93*, 022137.

(59) Kawata, S.; Sugiura, T. Movement of micrometer-sized particles in the evanescent field of a laser beam. *Opt. Lett.* **1992**, *17*, 772−774.

(60) Reece, P. J.; Garcés-Chávez, V.; Dholakia, K. Near-field optical micromanipulation with cavity enhanced evanescent waves. *Appl. Phys. Lett.* **2006**, *88*, 221116.

(61) Shilkin, D. A.; Lyubin, E. V.; Soboleva, I. V.; Fedyanin, A. A. Direct measurements of forces induced by Bloch surface waves in a one-dimensional photonic crystal. *Opt. Lett.* **2015**, *40*, 4883−4886.

(62) Liang, L.; Zuo, Y. F.; Wu, W.; Zhu, X. Q.; Yang, Y. Optofluidic restricted imaging, spectroscopy and counting of nanoparticles by evanescent wave using immiscible liquids. *Lab Chip* **2016**, *16*, 3007−3014.

(63) Harrick, N. J. Electric field strengths at totally reflecting interfaces. *J. Opt. Soc. Am.* **1965**, *55*, 851−857.

(64) Shilkin, D. A.; Lyubin, E. V.; Soboleva, I. V.; Fedyanin, A. A. Near-field probing of Bloch surface waves in a dielectric multilayer using photonic force microscopy. *J. Opt. Soc. Am. B* **2016**, *33*, 1120−1127.

(65) Green, M. A.; Keevers, M. J. Optical properties of intrinsic silicon at 300K. *Prog. Photovoltaics* **1995**, *3*, 189−192.

(66) Daimon, M.; Masumura, A. Measurement of the refractive index of distilled water from the near-infrared region to the ultraviolet region. *Appl. Opt.* **2007**, *46*, 3811−3820.

(67) Hale, G. M.; Querry, M. R. Optical constants of water in the 200-nm to 200-μm wavelength region. *Appl. Opt.* **1973**, *12*, 555−563.

(68) Jones, P.; Maragò, O.; Volpe, G. *Optical Tweezers: Principles and Applications*; Cambridge University Press, 2015.

■ NOTE ADDED AFTER ASAP PUBLICATION

This paper was originally published ASAP on August 22, 2017. Due to a production error, there was an error in eq 6. The corrected version was reposted on August 24, 2017.